Supporting Information

Dual Near Infrared Two-Photon Microscopy for Deep-Tissue Dopamine Nanosensor Imaging

Jackson T. Del Bonis-O'Donnell[1], Ralph H. Page[1], Abraham G. Beyene[1], Eric G. Tindall[1], Ian R. McFarlane[1], Markita P. Landry[1,2,3]*

[1] Chemical and Biomolecular Engineering, University of California, Berkeley, CA 94720
[2] California Institute for Quantitative Biosciences, QB3, University of California, Berkeley, CA 94720
[3] Chan-Zuckerberg Biohub, San Francisco, CA 94158

*E-mail: landry@berkeley.edu

Supplemental Background Information

Two parameters of fluorophores primarily influence the engineering of a two-photon-excited imaging/sensing system: fluorescence quantum efficiency Q_{1P}, and the two-photon-absorption cross section σ_{2P}. For a given fluorophore concentration (number density,) Q_{1P} governs the maximum brightness available as signal photons. This in turn affects the system signal-to-noise ratio (SNR) and the time required to take a measurement or to record an image. σ_{2P} sets the scale for the intensity that will just barely saturate the absorption of fluorophores at the laser's focal plane. Under-pumping reduces the number of signal photons (and SNR;) over-pumping generally increases the signal strength but degrades the imaging spatial resolution. The onset of saturation can be difficult to assess, thus modeling of its impact on both transverse and longitudinal spatial resolution has been reported.[1]

Estimates for Q_{1P}: Previous reports of Q_{1P} have ranged from slightly above 10^{-4},[2] to a few percent.[3] There are dramatic dependences on sample makeup and processing—aggregation, presence of "metallic" nanotubes, and host-medium properties all influence the radiationless-decay rate.

Estimates for σ_{2P}: Direct measurements of σ_{2P} for carbon nanotubes are scarce. Wang *et al.* performed two-photon excitation and adhered to a low-power regime in which the signal varied as the square of the laser fluence.[4] From their reported laser parameters, it can be inferred that σ_{2P} could not have exceeded 700,000 GM (note that 1 GM, the unit of two-photon absorption cross section, is defined as 10^{-50} cm⁴ sec/photon.) In Pomraenke *et al.*,[5] saturation of the (7,5) nanotube two-photon transition was observed as a change in slope (from 2 to 1) on a log-log plot of signal vs. laser power, as the power was increased. This puts a lower bound of 10,000 GM on σ_{2P}.

To obtain estimates of Q_{1P} and σ_{2P} for single-walled carbon nanotube (SWNTs,) nanosensors, we employed a reference dye solution (DTTC in DMSO) for which Q_{1P} and σ_{2P} are known,[6] and made relative measurements. One-photon pumping with a 633 nm He-Ne laser yielded an estimate of $Q_{1P} = 0.0023$ (assumed to be identical for one- and two-photon pumping.) Two-photon pumping with an ultrafast 1560 nm laser enabled measurement of σ_{2P} to be 239,000 GM (which depends on the derived value of Q_{1P}.)

Theoretical assessment of fluorescence quantum efficiency Q_{1P}, and the two-photon-absorption cross section σ_{2P}

Assessment of Q_{1P} is based on measurements of the absorbed one-photon pump power P_{abs} and fluorescence signal S, which is proportional to number of detected photons. Assuming various light-collection efficiencies etc. are identical for the DTTC and SWNT samples,

$$Q_{1P,S} = Q_{1P,R} \frac{S_{1P,S} n_{1P,S}^2 / (T_{1P,S} A_{1P,S})}{S_{1P,R} n_{1P,R}^2 / (T_{1P,R} A_{1P,R})} \quad (1)$$

where S is the number of photons detected in the integration period T with the absorbed fraction A of the impinging pump light on the sample whose refractive index is n. The refractive-index factors n account for refraction of the emitted fluorescence.[3e]

Measurement of the absorbed pump power is not realistic in the two-photon case. Instead, we assume that the two-photon-pumped volumes[7] are identical and rely on knowledge of the fluorophore number densities N to calculate the ratio

$$\sigma_{2P,S} = \sigma_{2P,R} \frac{S_{2P,S} n_{2P,S}^2 / (T_{2P,S} N_{2P,S} Q_{1P,S})}{S_{2P,R} n_{2P,R}^2 / (T_{2P,R} N_{2P,R} Q_{1P,R})} \quad (2)$$

Note that errors in $Q_{1P,S}$ propagate into the σ_{2P} estimate. Also, pumping below the onset of saturation is assumed.

NIR-EE fluorescence spectroscopy setup
The perpendicular-geometry fluorescence excitation/detection setup (**Figure 1b**, main text) includes a spectrophotometer cuvette mounted on a pair of translation stages that enable accurate placement with respect to the pump-beam waist. The pump light was focused with a 40 mm focal-length "best form" lens, and the beam skimmed the wall of the cuvette facing the spectrometer. The cuvette's face was imaged with near-unity magnification onto a Princeton Instruments SCT 320 spectrometer slit with a pair of 50 mm focal-length plano-convex lenses of 25 mm diameter. Accurate height alignment centers the image of the fluorescence stripe on the spectrometer slit, whose wavelength-dispersed image is in turn relayed to the PyLon-IR linear detector array with 0.5 mm pixel height. With a 150 groove/mm diffraction grating, the 1024-element detector array (with 25 µm pixel pitch and ~25 mm length) covers a ~ 500 nm wavelength region. The resultant ~20 nm / mm dispersion, coupled with typical ~1 – 2 mm slit widths, yields spectral resolutions on the order of tens of nm.

One-photon excitation of both DTTC and SWNT samples was accomplished with a ~ 5 mW CW 633 nm He-Ne laser whose beam radius at the focusing lens was on the order of 1 mm. To perform two-photon excitation, a Menlo Systems single-mode-fiber-pigtailed ELMO laser was used as the excitation source. Its nominal wavelength, repetition rate, and pulsewidth were respectively 1560 nm ± 30 nm, 100 MHz, and <90 fsec. Upon collimation and passage through a 5-power beam expander, the available average power was 77 mW. Aperture-transmission measurements[8] indicated a $1/e^2$ beam waist parameter of 4.1 mm. If focused in free space with a 40 mm lens, the focused waist radius and confocal distance is on the order of 5 µm and 100 µm, respectively.

SWNT and DTTC sample preparation
The SWNT samples – (GT)$_{15}$-SWNT and (6,5)-enriched-SWNT were prepared as detailed previously (See Materials and Methods section of main text). The near-IR dye DTTC dissolved in DMSO has been previously calibrated in terms of quantum yield and 1.55 µm two-photon-absorption cross section.[6] Our DTTC reference solutions were prepared at a concentration of

50 µM for two-photon excitation fluorescence measurements, and approximately 5 µM for one-photon-excitation quantum yield measurements.

SWNT sample concentrations were determined using UV-Vis-IR absorption spectrometry. Absorption spectra of the SWNT and DTTC solutions in cuvettes were recorded on a Shimadzu model 3600 Plus UV-VIS-NIR spectrophotometer. Separate recordings of solvent (respectively 2% SDS in deionized water, and DMSO) spectra enabled baseline subtraction. Our measurements yielded SWNT sample concentrations of 0.76 mg L^{-1} for all (6,5) SDS SWNT suspension experiments (see **Table S4**). (GT)$_{15}$ SWNT concentrations were calculated using measured absorbance at 632 nm and extinction coefficient of ε=0.036 L mg^{-1} cm^{-1}.[9]

Calibrations and quantum yield measurements
To evaluate S, the signal proportional to the number of detected photons, it is necessary to correct for the wavelength-dependent spectrometer response $R(\lambda)$. A blackbody-source was used for spectrometer calibration, with the photon flux rate assumed to vary as[10]

$$F_{BB}(\lambda) = F_0\big(\lambda^{-4}e^{(hc/\lambda kT)} - 1\big)^{-1} \quad (3)$$

where F_0 is a constant, λ is wavelength, h is Planck's constant, k is Boltzmann's constant, c is the speed of light and T is the temperature of the source.

A 100 watt GE soft-white light bulb was positioned approximately 10 cm from the spectrometer slit, with slit width set to 100 microns. The light bulb's filament temperature was 2550° C (2823 K).[11] Using the 150 groove/mm grating, spectra were recorded for center wavelengths of 1000 and 1100 nm to match the settings employed while recording DTTC and SWNT spectra. In this spectral region, the light bulb's glass envelope is not expected to influence the spectrum significantly. Impact on Q_{1P} and σ_{2P} is expected to be at the few-percent level because the light bulb's emission is stronger in the infrared than in the visible, and because the InGaAs detector array is comparatively insensitive in the visible region. Because the blackbody curve is gently sloped in the region of interest, an error in filament temperature also has a mild effect on the results.

Figure S3a shows an absorption spectrum of a (6,5)-enriched SWNT sample in water and 2% SDS. The well-known SWNT absorption peaks at 990 and 574 nm are clearly identifiable.[12] According to this data, the optical density at the 633 nm He-Ne laser wavelength is 0.142, corresponding to 26.9% single-pass absorption for a 1 cm path length. **Figure S3b** is the corresponding spectrum of a 5 µM solution of DTTC in DMSO. On the short-wavelength shoulder of the 770 nm transition, the 633 nm optical density is 0.028, yielding 6.2% single-pass absorption in a 1 cm path.

Raw emission spectra $I_{raw}(\lambda)$ for the two samples are shown in **Figure S4**. Despite a low concentration and low 633 nm absorption, the DTTC solution, whose emission quantum yield is 64%,[6] gave a strong signal, and its spectrum was recorded with a 1 sec integration time and 1 mm slit setting. For the SWNT solution, the detector integration time was set to 1 sec, and the presented spectrum represents the average of four scans. Its ~20 nm width is consistent with the 1 mm slit setting and 20 nm/mm spectrometer dispersion. Spectrometer center-wavelength settings for the two spectra are 1000 nm and 1100 nm, respectively.

White-light calibration data $I_{bulb}(\lambda)$ for the 1000 nm and 1100 nm center spectrometer setting (150 groove/mm grating) are shown in **Figure S6 and S7** respectively, which contain the raw

spectra and a 2550 °C blackbody curve. According to the InGaAs array quantum-efficiency curve, the response is nearly constant from 1000 to 1600 nm, declines sharply at 1700 nm, and declines sharply in the visible region. Thus, the response in the 800 – 1200 nm region is dominated by the diffraction-grating efficiency. We calculate the system responsivity $R(\lambda)$ curve in **Figure S4b** by subtracting a 600-count dark-current offset ($I_{background}$) from the raw spectrum $I_{bulb}(\lambda)$ and then take the ratio $(I_{raw}(\lambda)-I_{background}(\lambda))/F_{BB}(\lambda)$. When corrected for dark-current offsets and wavelength-dependent response $R(\lambda)$, the raw spectra $I_{raw}(\lambda)$ of **Figure S4** appear as in **Figure S8**. These are the spectra that are integrated to determine the relative numbers of detected photons S:

$$S = \int I_{raw}(\lambda)/R(\lambda)d\lambda \quad (4)$$

Upon responsivity normalization, the DTTC spectrum grows in prominence with respect to the SWNT spectrum. The limits of integration for the DTTC and SWNT spectra were respectively 750 – 1150 nm and 850 – 1250 nm. Thus, the 1270 nm scattered He-Ne laser signal did not contribute to the fluorescence spectra. **Table S3** summarizes the parameters used as input data for Equation (1) and includes the derived Q_{1P} value of 0.0023 for the (6,5)-enriched SWNT solution. This value is within the $Q_{1P} = 0 – 1\%$ range reported by Crochet, *et al.*[3e] for a suite of ultra-centrifuged samples, and close to the reported $Q_{1P} \sim 0.25\%$ ensemble average.

The effect of varying the assumed temperature of the blackbody calibration lamp is modest. Given our present experimental spectra, the change in Q_{1P} caused by a 100 °K change is less than 4%. Uncertainties in optical densities, DTTC quantum yield, and other factors most likely combine to cause Q_{1P} to be uncertain at the several-tens-of-percent level.

Calculating 2PE cross sections
For the fluorescence quantum yield, emission spectra for SWNT and DTTC samples can be integrated and ratioed to compute the relative two-photon-absorption cross section. In the case of one-photon absorption, monitoring the rate of pump-photon absorption is straightforward. With two-photon absorption, it is more reliable to determine the number of fluorophores in the effective volume V_2 that contributes to the fluorescence signal:[7]

$$V_2 = \frac{4}{3}n_0 \frac{\pi^3 \omega_0^4}{\lambda} \quad (5)$$

Because the laser-spot radius ω_0 governs the confocal distance (i.e. depth of focus) $b = 2\pi\omega_0^2/\lambda$, V_2 can be interpreted as (spot area)*(depth of focus). Owing to refraction, the depth of focus is elongated by the factor n_0, the medium refractive index.

Several nuances contribute to our estimates of SWNT number density. First, SWNT samples constitute a distribution of SWNT lengths, which contributes to the number of excitons each SWNT supports. We thus employ as a benchmark the average distance over which an exciton diffuses prior to recombination (radiative or otherwise). Calibrated measurements on SWNT absorption spectra[13] show that for "long" SWNTs, each carbon atom contributes a certain amount of oscillator strength to the exciton absorption peak. Thus, we can straightforwardly determine the C-atom concentration C_C of a SWNT solution, from its absorption spectrum. With knowledge of the C-atom linear density and assumed "exciton length" of the chirality under consideration, we allocate a certain number of carbon atoms to each "effective nanotube" and derive the fluorophore concentration.

4

Schöppler et al.[12] have investigated the (6,5) chirality SWNT exciton absorption peaks and find for the 990 nm (fundamental) transition, a decadal (base 10) extinction coefficient of 4400 cm^{-1} mol C atoms^{-1} liter.) Furthermore, the (6,5) chirality nanotube's carbon-atom linear density is 88 nm^{-1}. Therefore, for the (6,5)-enriched sample measured with a 1-cm path length:

$$C_{\mathrm{C}} = \frac{OD_{990}}{4400} \ [\mathrm{M}] \quad (6)$$

Assuming an effective nanotube length L [nm] that supports a single exciton, the corresponding nanotube concentration becomes:

$$N = \frac{C_{\mathrm{C}}}{88L} \ [\mathrm{M}] \quad (7)$$

Values reported for SWNT exciton diffusion lengths range from 2 to 13 nm, and depend on the medium in which the nanotubes are immersed.[13] For our calculations, we choose a lower-bound of 2 nm exciton diffusion presuming that sample inhomogeneities will modulate the electrostatic potential, and act to limit exciton diffusion. σ_{2P} depends proportionally on the value chosen for L. Based on the SWNT-sample absorption spectrum (**Figure S2a**) whose optical density at the 990 nm exciton peak is 0.30, the C atom concentration is 64 µM. With a nanotube effective length of 2 nm as per each exciton length, the derived (6,5) nanotube concentration is 3.6 x 10^{-7} M.

Uncorrected two-photon-emission spectra obtained with the 1560 nm ELMO laser are shown in **Figure S5**. Corresponding spectra, corrected for wavelength-dependent response using the data of **Figures S6b** and **S7b**, are shown in **Figure S9**. The dominance of a single emission peak near 975 nm in the SWNT spectrum is evidence of the high enrichment of a single chirality. Integrals of these spectra in the wavelength ranges 750 - 1150 nm (DTTC) and 850 - 1250 nm (SWNT) are reported in **Table S4** and used in **Equation 2** to derive the SWNT two-photon-absorption cross section of 239,000 GM. According to Wang et al.,[4] the 1560 nm laser wavelength is resonant with the (6,5) two-photon transition at 1.59 eV. Two-photon-excitation spectra of me Maultzsch et al.[13f] and Pomraenke et al.[5] center the (6,5) transition peak at ~1650 nm, corresponding to an energy ~1.50 eV. The discrepancy arises from differences in the nanotube environment: SWNT from Wang et al. were prepared in a dry polymer matrix of poly(maleic acid/octyl vinyl ether), whereas the other studies prepared SWNT in aqueous solutions of the surfactant SDS. We conclude that the 1560 nm wavelength probed either the peak exciton cross section, or a value roughly half the peak, corresponding to higher-energy excitation.[4]

Calibration lamp temperature and SWNT length contributions
The SWNT fluorescence quantum yield Q_{1P} enters parametrically into the calculation of the two-photon absorption cross section, σ_{2P} above. Thus, ratios of integrated, wavelength-response-corrected spectra are involved in two instances. Therefore, the wavelength-response-calibration biases applied to both the one- and two-photon data sets will nearly cancel if the emission spectra are similar for both SWNT samples, as in our case (**Figure 2**, main text). Thus, ignoring wavelength-independent factors in equations (1) and (2):

$$\frac{\sigma_{2P,S}}{\sigma_{2P,R}} \sim \frac{\int I_{2P,S,raw}/R(\lambda)d\lambda}{\int I_{2P,R,raw}/R(\lambda)d\lambda} \frac{\int I_{1P,R,raw}/R(\lambda)d\lambda}{\int I_{1P,S,raw}/R(\lambda)d\lambda} \qquad (8)$$

$I_{1P,raw}$ and $I_{2P,raw}$ are respectively the raw spectra obtained with one- and two-photon pumping. Given the 2 nm choice for L, our result for $\sigma_{2P,SWNT}$ lies within the 10,000 – 700,000 GM bounds estimated from the reports of Wang *et al.* and Pomraenke *et al.* Errors in $R(\lambda)$ cancel if $I_{1P,raw}$ is proportional to $I_{2P,raw}$. Whereas a 100 °K change of the assumed calibration-lamp temperature shifted Q_{1P} by 3 – 4%, the effect on σ_{2P} is less than 0.3%

In addition to the effective nanotube length, which we approximate as the exciton diffusion length, the absorption cross section used to establish the carbon-atom number density contributes uncertainty to our measurements.[14] Techniques employed by Schöppler *et al.*[12] report cross sections differing by a factor of 2 for the S_1 transition, reporting an average of 1.7 x 10^{-17} cm^2 per carbon atom, yielding a molar extinction coefficient of 4400 cm^{-1} M^{-1}. For the weaker S_2 transition, the reported molar extinction coefficient is ~ 1500 cm^{-1} M^{-1}. Separating the contributions to $\sigma^{(1)}$ arising from the exciton and continuum transitions is achieved by curve-fitting. Oudjedi *et al.*[15] have since reported for the S_2 transition an absorption cross section $\sigma^{(1)}$ of 3.2 x 10^{-17} cm^2 per carbon atom, which translates to a molar extinction coefficient $N_A \sigma^{(1)}$ /1000 ln(10) ~ 8400 cm^{-1} M^{-1}. The fivefold difference in these values suggests that the uncertainty in σ_{2P} values is at the order-of-magnitude level.

Consideration of absolute signal levels for microscopy
The estimated C-atom concentration of our (6,5)-enriched sample of 6.4 x 10^{-5} M corresponds to a mass density of 0.76 mg L^{-1}. Under the gentle focusing conditions used, the two-photon signal (integrated over the 900 – 1300 nm spectral range) was ~ 30,000 counts per second on the detector array using high gain. In this configuration, it takes roughly 80 photoelectrons to produce a count, and over much of the spectral range, the InGaAs quantum efficiency is ~0.8. Thus, each count represents the impingement of ~100 photons on the detector array. Consequently, our count rate of 3 x 10^4 sec^{-1} implies a signal-photon-collection rate of ~ 3 x 10^6 sec^{-1}.

Under our focusing conditions (40 mm focal length, and 4.1 mm input beam waist parameter, using 1.55 μm light) the focused waist ω_0 is estimated to be 4.8 μm. With a medium (water) refractive index n_0 near 1.3, the effective volume (Equation 5) is 18,600 μm^3. At this modest spatial resolution, the multi-kHz count rate would enable production of an image with useful signal-to-noise ratio with few-msec pixel dwell times.

The expected count rate drops rapidly as higher spatial resolution is sought. For example, reduction of ω_0 to 1.0 μm shrinks V_2 to ~ 35 μm^3. Concomitant reduction of the photon-collection rate to ~ 5600 sec^{-1} would be expected, and corresponds to a ~ 56 sec^{-1} photon count rate using our detector. Pixel dwell times on the order of 1 sec might be needed for imaging in this scenario.

We expect that this signal strength, and consequently the pixel dwell time, can be improved through configuration and hardware considerations. For example, using a high-numerical-aperture light-collection systems would provide significant signal improvement compared to the relatively modest f/4.6 aperture ratio used here.
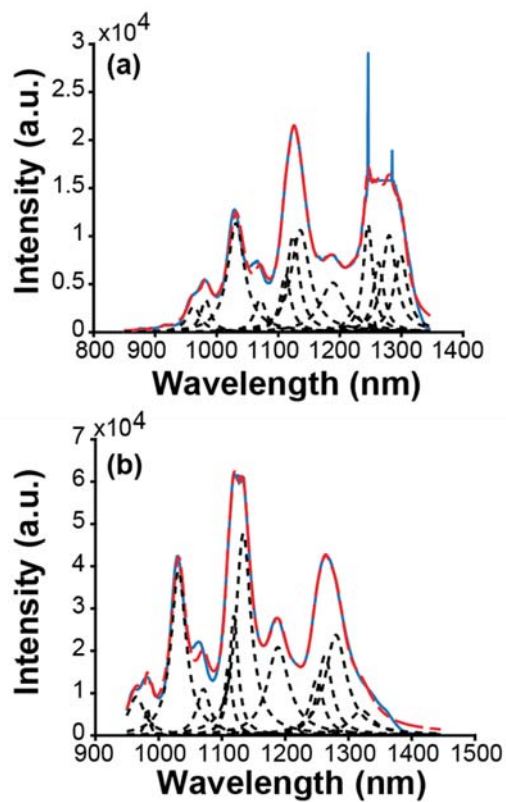
Figure S1. The deconvolution of fluorescence emission spectra for (GT)$_{15}$-DNA SWNT nanosensors into individual chirality components using one-photon excitation (a) prior to dopamine addition, and (b) after dopamine addition. The solid blue line is the original spectrum and the dashed red line is the sum of the individual chirality components calculated using a non-linear least squares method.

Figure S2. The deconvolution of fluorescence emission spectra using for $(GT)_{15}$-DNA SWNT nanosensors into individual chirality components using two-photon excitation (a) prior to dopamine addition, and (b) after dopamine addition. The solid blue line is the original spectrum and the dashed red line is the sum of the individual chirality components calculated using a non-linear least squares method.
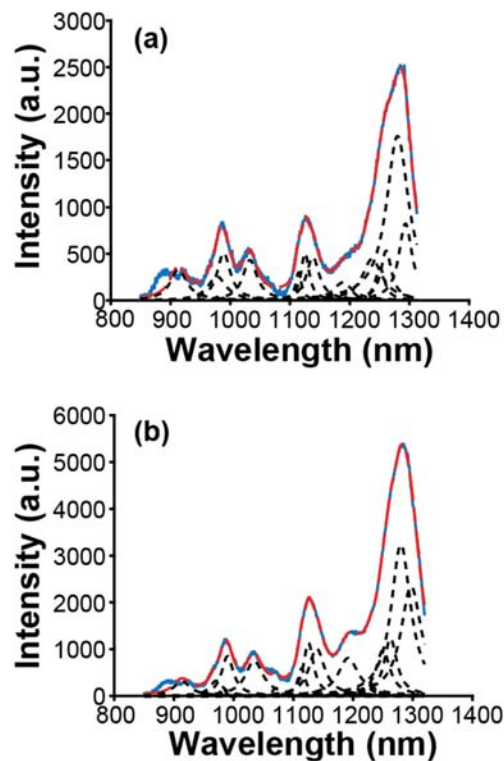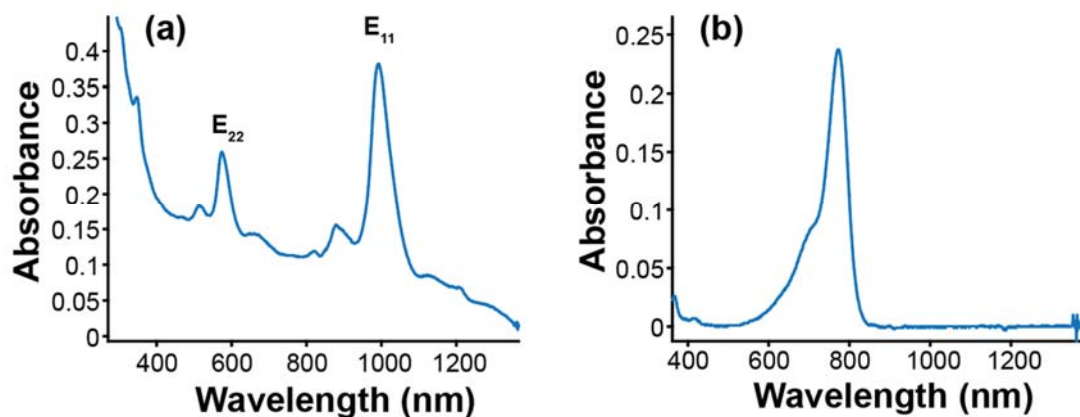

Figure S3. Absorption spectra for 10 mm path lengths of (a) a (6,5)-enriched SWNT in a 2% SDS aqueous solution (b) a <5 µM solution of DTTC in DMSO.

Figure S4. Raw emission spectra $I_{raw}^{(1)}(\lambda)$ (uncorrected for wavelength-dependent spectrometer response) of (a) (6,5) – enriched SWNT sample and (b) DTTC reference solution, pumped with a 5 mW 633 nm He-Ne laser with an integration times of 1 sec.
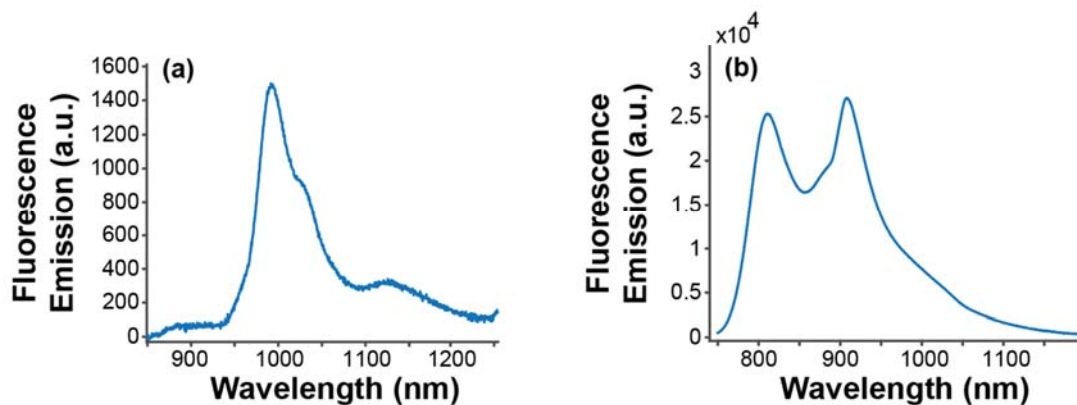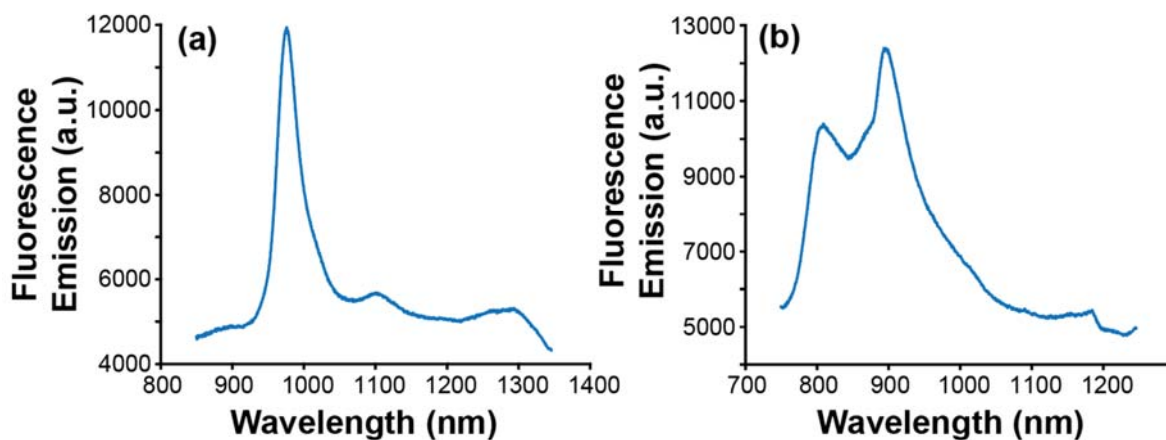

Figure S5. Raw emission spectra $I_{raw}^{(2)}(\lambda)$ (uncorrected for baseline offset and wavelength-dependent spectrometer response) of (a) (6,5) –enriched SWNT sample and (b) DTTC reference solution, pumped with a focused 77 mW, 100 MHz rep rate, 1560 nm sub-psec laser with integrations times of 30 s and 10 s respectively.

9
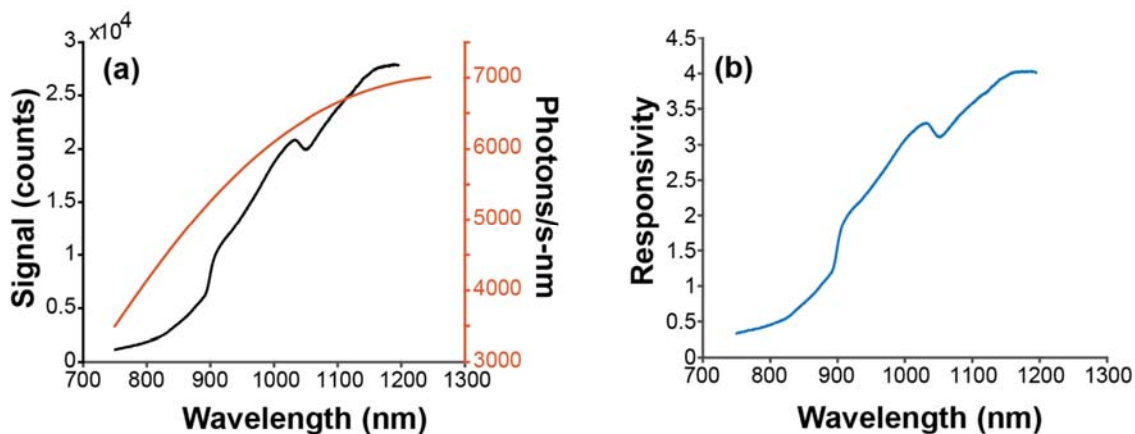
Figure S6. (a) Raw wavelength-response-calibration spectrum $I_{bulb}(\lambda)$ obtained with 100 W soft-white light bulb and spectrometer center wavelength of 1000 nm. A scaled blackbody curve $F_{BB}(\lambda)$ (photon sec^{-1} nm^{-1}) corresponding to 2550 °C is superimposed and set to an arbitrary scale. (b) Derived responsivity curve $R(\lambda)$ for 1000 nm center wavelength.
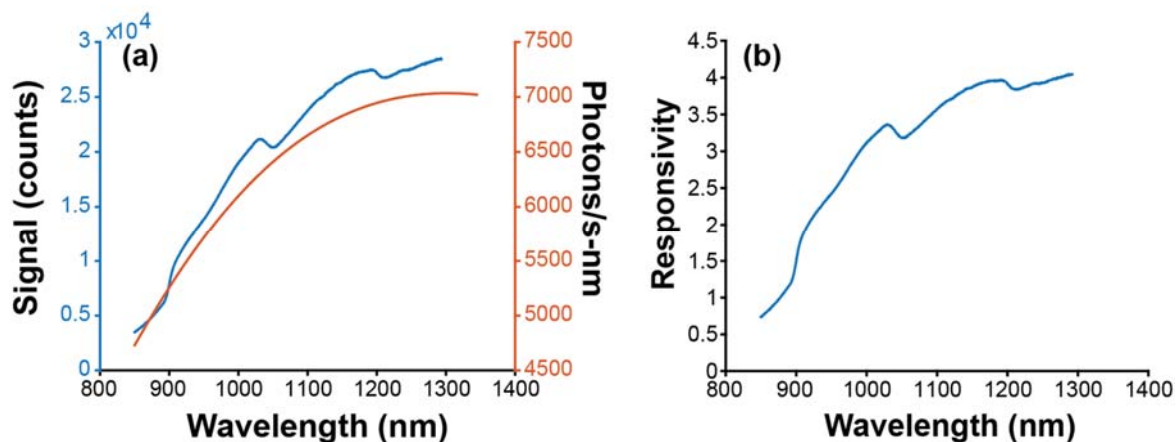
Figure S7. As in Figure S6, for 1100 nm spectrometer center wavelength.

Figure S8. Wavelength-response-corrected emission spectra (of Figure S4) for (a) (6,5)-enriched SWNT sample and (b) DTTC / DMSO solution excited using the 633 nm HeNe source.

Figure S9. Wavelength-response-corrected two-photon-pumped emission spectra (of Figure S7) for (a) (6,5)-enriched SWNT sample and (b) DTTC / DMSO solution using the 1560 nm excitation source.

focal
volume

pixel array
0.5 mm

cuvette
image

2 mm
slit width

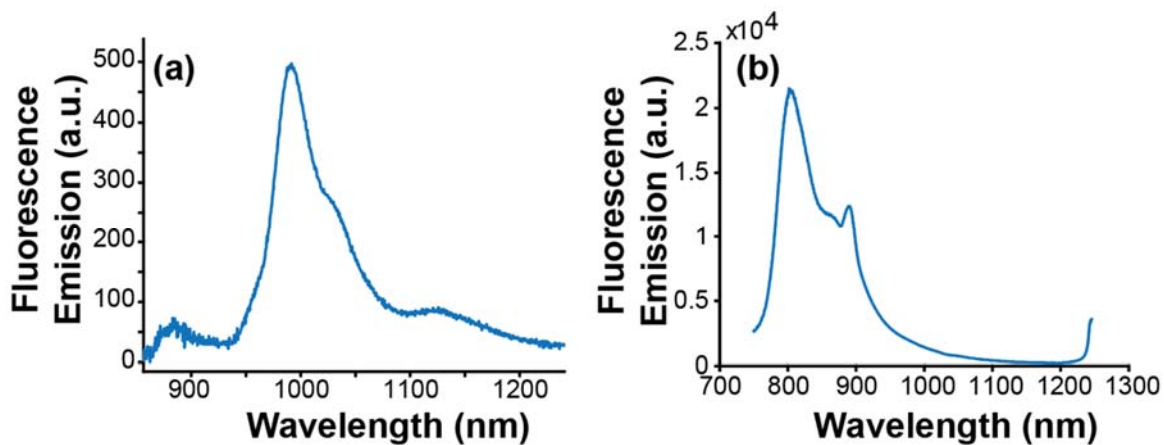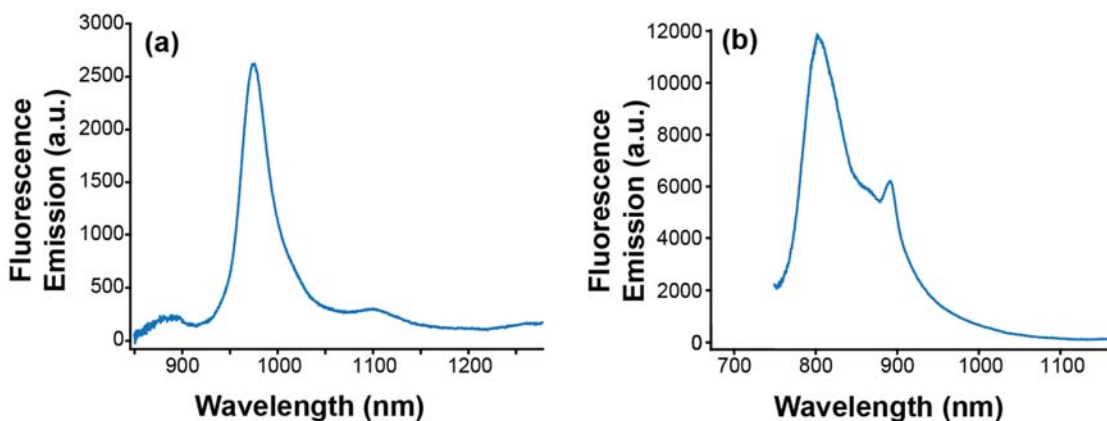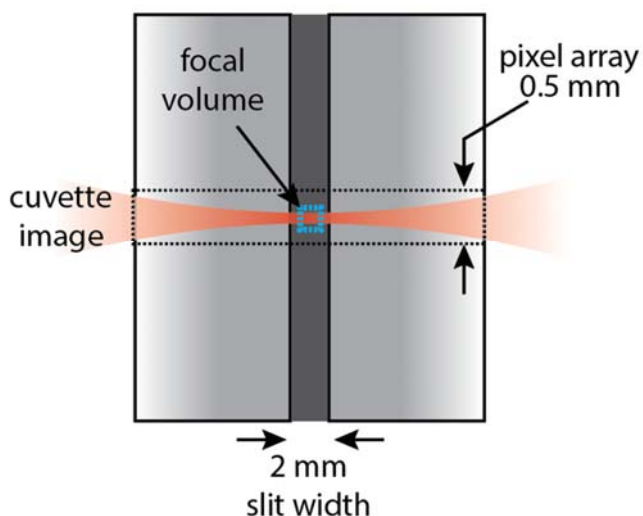**Figure S10.** Imaging of scattered light and fluorescence from the sample cuvette onto the spectrometer slit whose wavelength-dispersed image is relayed to the InGaAs detector array. In the one-photon-excitation case, the stripe of fluorescent light is ~10 mm long (corresponding to the cuvette's interior dimension,) and over-fills the slit of width ~ 2 mm. With a focused Gaussian beam and two-photon excitation, the fluorescent zone length is on the order of the Rayleigh range (well under 1 mm.)

Table S1. Deconvolution parameters calculated for Figure S1a. $(GT)_{15}$-DNA wrapped SWNTs emission spectra for one-photon excitation.

n	m	center	peak height	FWHM	area	error	Group Sum
9	1	914.243	210.649	12.755	4225.316	0.988	285719.797
8	3	962.625	2684.545	34.67	146211.43	0.988	
6	5	982.158	3343.418	25.748	135283.051	0.988	
7	5	1031.349	11335.268	38.465	684893.972	0.988	684893.972
10	2	1070.674	3418.079	25.084	134694.695	0.988	134694.695
9	4	1111.54	6030.799	20.467	193918.517	0.988	1149948.776
7	6	1135.7	10616.916	34.943	582839.412	0.988	
8	4	1123.99	10066.299	23.596	373190.847	0.988	
8	6	1188.497	5143.903	43.098	348249.324	0.988	425868.32
12	1	1188.497	0.143	41.455	9.335	0.988	
11	3	1221.925	2147.909	23.003	77609.661	0.988	
8	7	1280.081	10072.605	20.908	330812.666	0.988	1025445.046
10	5	1255.575	1212.632	3.912	7452.37	0.988	
9	5	1245.69	11215.355	14.774	260384.414	0.988	
10	3	1262.731	7243.955	16.042	182547.884	0.988	
12	2	1298.621	8030.694	19.361	244247.712	0.988	
0	0	982	0	11	0.008	0.988	

Table S2. Deconvolution parameters calculated for Figure S2a. (GT)$_{15}$-DNA wrapped SWNTs emission spectra for two-photon excitation.

n	m	center	peak height	FWHM	area	error	Group Sum
9	1	913.224	331.88	50	26066.919	0.994	72355.584
8	3	977.649	257.106	47.533	19198.843	0.994	
6	5	988.97	510.037	33.802	27089.822	0.994	
7	5	1032.817	433.383	33.622	22888.569	0.994	22888.569
10	2	1070.674	0	47.587	0	0.994	
9	4	1114.352	299.785	11.839	5582.977	0.994	36637.513
7	6	1138.23	466.756	24.802	18185.918	0.994	
8	4	1125.305	509.057	16.093	12868.618	0.994	
8	6	1204.705	85.268	15.41	2064.378	0.994	12903.197
12	1	1188.497	191.937	33.699	10160.713	0.994	
11	3	1221.925	16.549	26.086	678.106	0.994	
8	7	1280.081	1758.027	34.522	95333.114	0.994	166613.319
10	5	1237.523	444.808	32.434	22663.978	0.994	
9	5	1250.598	352.062	15.088	8347.235	0.994	
10	3	1261.027	532.305	17.032	14243.932	0.994	
12	2	1293.366	825.259	20.075	26025.06	0.994	
0	0	982	69.637	11	1204.313	0.994	

Table S3. Parameters pertaining to determination of (6,5)-enriched SWNT quantum yield.

Parameter	Symbol [units]	DTTC / DMSO	SWNT / H$_2$O / SDS
Refractive index	n	1.47	1.33
633 nm optical density		0.028	0.142
Pump absorption	A [%]	6.2	26.9
Integrated signal S	S [counts]	4,765,051	95,229
Integration time T	T [sec]	1	1
Quantum yield	Q_{1P}	0.64 [6]	0.0023 [this work]

Table S4. Parameters pertaining to determination of (6,5)-enriched SWNT two-photon-absorption cross section.

Parameter	Symbol [units]	DTTC / DMSO	SWNT / H$_2$O / SDS
Refractive index	n	1.47	1.33
990 nm optical density		N/A	0.28
C-atom concentration	C_C [M]	N/A	6.4 x 10^{-5}
Nanotube effective length	L [nm]	N/A	2
Fluorophore concentration	N [M]	50 x 10^{-6}	3.6 x 10^{-7}
Integrated signal S	S [counts]	2,554,399	363,725
Integration time T	T [sec]	10	30
Quantum yield	Q_{1P}	0.64 [6]	0.0023 [this work]
2-photon cross section	σ_{2P} [GM]	160 [6]	239,000 [this work]

Table S5. Deconvolution parameters calculated for Figure S1b. (GT)$_{15}$-DNA wrapped SWNTs emission spectra for one-photon excitation after adding dopamine.

n	m	center	peak height	FWHM	area	error	Group Sum
9	1	0	0	0	0	0	636416.135
8	3	964.615	9135.672	42.016	602951.289	0.994	
6	5	989.067	2900.892	7.32	33464.846	0.994	
7	5	1031.349	38955.573	33.206	2032290.811	0.994	2032290.811
10	2	1070.674	10953.679	27.802	478414.683	0.994	478414.683
9	4	1109.973	16241.872	15.121	385781.636	0.994	3187932.347
7	6	1133.739	47711.998	27.825	2085522.247	0.994	
8	4	1118.765	28219.097	16.167	716628.464	0.994	
8	6	1188.497	20842.375	36.585	1197806.388	0.994	1233446.233
12	1	1188.498	1.695	36.472	97.129	0.994	
11	3	1217.884	1647.09	13.737	35542.716	0.994	
8	7	1280.081	23731.299	30.952	1153877.326	0.994	2514805.571
10	5	1262.731	18780.126	21.502	634398.733	0.994	
9	5	1249.588	13224.926	20.421	424330.962	0.994	
10	3	1261.974	0.019	23.31	0.681	0.994	
12	2	1320.925	5881.001	32.711	302197.869	0.994	
0	0	982	6670.28	11	115416.05	0.994	

Table S6. Deconvolution parameters calculated for Figure S2b. (GT)$_{15}$-DNA wrapped SWNTs emission spectra for two-photon excitation after adding dopamine.

n	m	center	peak height	FWHM	area	error	Group Sum
9	1	913.224	315.855	50	24808.266	0.998	83578.623
8	3	970.804	323.337	34.974	17767.659	0.998	
6	5	989.682	850.254	30.7	41002.698	0.998	
7	5	1034.378	749.891	41.907	49367.173	0.998	53278.88
10	2	1070.674	172.993	14.39	3911.707	0.998	
9	4	1113.883	588.809	15.441	14291.964	0.998	98570.197
7	6	1139.063	1014.337	30.39	48431.738	0.998	
8	4	1125.338	1134.487	20.114	35846.495	0.998	
8	6	1207.928	145.886	17.571	4026.575	0.998	56351.099
12	1	1191.93	813.587	35.95	45944.254	0.998	
11	3	1221.925	196.411	20.68	6380.27	0.998	
8	7	1280.081	3236.224	30.077	152893.159	0.998	346407.462
10	5	1250.146	980.498	22.516	34682.338	0.998	
9	5	1231.642	258.247	15.938	6465.647	0.998	
10	3	1262.731	1230.323	20.102	38849.862	0.998	
12	2	1297.224	2343.359	30.839	113516.456	0.998	
0	0	982	194.44	11	3362.651	0.998	

References

[1]   G. Cianci, J. Wu, K. Berland, *Microsc. Res. Tech.* **2004**, *64*, 135-141.

[2]   F. Wang, G. Dukovic, L. E. Brus, T. F. Heinz, *Phys.l Rev. Lett.* **2004**, *92*, 177401.

[3]   a) T. K. Cherukuri, D. A. Tsyboulski, R. B. Weisman, *ACS Nano* **2012**, *6*, 843-850; b) T. Hertel, S. Himmelein, T. Ackermann, D. Stich, *ACS Nano* **2010**, *12*, 7161-7168; c) Lisa J. Carlson, Sara E. Maccagnano, Ming Zheng, John Silcox, Todd D. Krauss, *Nano Lett.* **2007**, *12*, 3698-3703; d) J. Lefebvre, D. G. Austing, J. Bond, P. Finnie, *Nano Lett.* **2006**, *6*, 1603–1608; e) J. Crochet, M. Clemens, T. Hertel, *J. Am. Chem. Soc.* **2007**, *129*, 8058-8059.

[4]   F. Wang, G. Dukovic, L. E. Brus, T. F. Heinz, *Science* **2005**, *308*, 838-840.

[5]   R. Pomraenke, J. Maultzsch, S. Reich, E. Chang, D. Prezzi, A. Ruini, E. Molinari, M. S. Strano, C. Thomsen, C. Lienau, *physica status solidi (b)* **2006**, *243*, 2428-2435.

[6]   M. Y. Berezin, C. Zhan, H. Lee, C. Joo, W. J. Akers, S. Yazdanfar, S. Achilefu, *J. Phys. Chem. B* **2011**, *115*, 11530-11535.

[7]   C. Xu, W. W. Webb, in *Topics in fluorescence spectroscopy*, Springer, **2002**, pp. 471-540.

[8]   A. Siegman, *Lasers*, University Science Books, Mill Valley, CA, **1986**.

[9]   S. Kruss, M. P. Landry, E. Vander Ende, B. M. a. Lima, N. F. Reuel, J. Zhang, J. Nelson, B. Mu, A. Hilmer, M. Strano, *J. Am. Chem. Soc.* **2014**, *136*, 713-724.

[10]   W. Driscoll, *Handbook of Optics*, McGraw-Hill, New York, NY, **1978**.

[11]   D. Klipstein, **2006**.

[12]   F. Schoppler, C. Mann, T. Hain, F. Neubauer, G. Privitera, F. Bonaccorso, D. Chu, A. Ferrari, T. Hertel, *J. Phys. Chem. C* **2011**, *115*, 14682-14686.

[13]   a) C. Mann, T. Hertel, *J. Phys. Chem. Lett.* **2016**, *7*, 2276-2280; b) Y. Miyauchi, H. Hirori, K. Matsuda, Y. Kanemitsu, *Phys. Rev. B* **2009**, *80*, 081410; c) Y. Miyauchi, *J. Mat. Chem. C* **2013**, *1*, 6499-6521; d) L. Luer, S. Hoseinkhani, D. Polli, J. Crochet, T. Hertel, G. Lanzani, *Nat. Photonics* **2009**, *5*, 54-58; e) R. Capaz, C. Spataru, S. Ismail-Beigi, S. Louie, *Phys. Rev. B* **2006**, *74*; f) J. Maultzsch, R. Pomraenke, S. Reich, E. Chang, D. Prezzi, A. Ruini, E. Molinari, M. S. Strano, C. Thomsen, C. Lienau, *Phys. Rev. B* **2005**, *72*, 241402-241402; g) V. Perebeinos, J. Tersoff, P. Avouris, *Phys. Rev. Lett.* **2004**, *92*, 257402; h) M. Hofmann, J. Noe, A. Kneer, J. Crochet, A. Hogele, *Nano Lett.* **2016**, *16*, 2958-2962; i) X. Ma, O. Roslyak, J. Duque, X. Pang, S. Doorn, A. Piryatinski, D. Dunlap, H. Htoon, *Phys. Rev. Lett.* **2015**, *115*, 017401; j) M. Iwamura, N. Akizuki, Y. Miyauchi, S. Mouri, J. Shaver, Z. Gao, L. Cognet, B. Lounis, K. Matsuda, *ACS Nano* **2014**, *8*, 11254-11260; k) D. Harrah, J. Schneck, A. Green, M. Hersam, L. Ziegler, A. Swan, *ACS Nano* **2011**, *5*, 9898-9906.

[14]   a) S. Sanchez, S. Bachilo, Y. Kadria-Vili, C. Lin, R. Weisman, *Nano Lett.* **2016**, *16*, 6903-6909; b) J. Streit, S. Bachilo, S. Ghosh, C. Lin, R. Weisman, *Nano Lett.* **2014**, *14*, 1530-1536; c) K. Liu, X. Hong, S. Choi, C. Jin, R. Capaz, J. Kim, W. Wang, X. Bai, S. Louie, E. Wang, F. Wang, *Proc. Natl. Acad. Sci. U.S.A.* **2014**, *111*, 7564-7569; d) E. Verdenhalven, E. Malic, *J. Phys.: Condens. Matter* **2013**, *25*; e) S. Choi, J. Deslippe, R. Capaz, S. Louie, *Nano Lett.* **2013**, *13*, 54-58.

[15]   L. Oudjedi, A. Parra-Vasquez, A. Godin, L. Cognet, B. Lounis, *J. Phys. Chem. Lett.* **2013**, *4*, 1460-1464.